Climatology of the Elevated Mixed Layer over the Contiguous United States and Northern Mexico Using ERA5: 1979–2021

MARGO S. ANDREWS,[a] VITTORIO A. GENSINI,[a] ALEX M. HABERLIE,[a] WALKER S. ASHLEY,[a] ALLISON C. MICHAELIS,[a] AND MATEUSZ TASZAREK[b]

[a] *Department of Earth, Atmosphere, and Environment, Northern Illinois University, DeKalb, Illinois*
[b] *Department of Meteorology and Climatology, Adam Mickiewicz University, Poznań, Poland*

(Manuscript received 29 August 2023, in final form 30 December 2023, accepted 3 January 2024)

ABSTRACT: Elevated mixed layers (EMLs) influence the severe convective storm climatology in the contiguous United States (CONUS), playing an important role in the initiation, sustenance, and suppression of storms. This study creates a high-resolution climatology of the EML to analyze variability and potential changes in EML frequency and characteristics for the first time. An objective algorithm is applied to ERA5 to detect EMLs, defined in part as layers of steep lapse rates (≥8.0°C km^{-1}) at least 200 hPa thick, in the CONUS and northern Mexico from 1979 to 2021. EMLs are most frequent over the Great Plains in spring and summer, with a standard deviation of 4–10 EML days per year highlighting sizable interannual variability. Mean convective inhibition associated with the EML's capping inversion suggests many EMLs prohibit convection, although—like nearly all EML characteristics—there is considerable spread and notable seasonal variability. In the High Plains, statistically significant increases in EML days (4–5 more days per decade) coincide with warmer EML bases and steeper EML lapse rates, driven by warming and drying in the low levels of the western CONUS during the study period. Additionally, increases in EML base temperatures result in significantly more EML-related convective inhibition over the Great Plains, which may continue to have implications for convective storm frequency, intensity, severe perils, and precipitation if this trend persists.

SIGNIFICANCE STATEMENT: Elevated mixed layers (EMLs) play a role in the spatiotemporal frequency of severe convective storms and precipitation across the contiguous United States and northern Mexico. This research creates a detailed EML climatology from a modern reanalysis dataset to uncover patterns and potential changes in EML frequency and associated meteorological characteristics. EMLs are most common over the Great Plains in spring and summer, but show significant variability year-to-year. Robust increases in the number of days with EMLs have occurred since 1979 across the High Plains. Lapse rates associated with EMLs have trended steeper, in part due to warmer EML base temperatures. This has resulted in increasing EML convective inhibition, which has important implications for regional climate.

KEYWORDS: Synoptic climatology; Severe storms; Climate variability

1. Introduction and background

The elevated mixed layer's (EML's) influence on the severe convective storm (SCS) climatology in the contiguous United States (CONUS) was identified nearly seven decades ago by Fawbush and Miller (1954). A function of the unique combination of topography and airmass source regions present in North America, the EML originates as a well-mixed ($d\theta/dz \approx 0$), deep planetary boundary layer (PBL) with high potential temperature due to intense surface heating over the elevated terrain of northern Mexico, the southwestern CONUS, the High Plains, and/or the Rocky Mountains (Carlson and Ludlam 1968; Carlson et al. 1983; Lanicci and Warner 1991a). Under certain synoptic patterns, this air mass is advected eastward and loses connection with the ground, flowing over and "capping" maritime tropical low-level flow that often originates over the Gulf of Mexico (Carlson et al. 1983; Lanicci and Warner 1991a). The EML is, therefore, an elevated air mass featuring nearly dry adiabatic lapse rates and relatively high potential temperature, typically with a capping inversion at its base (Carlson and Ludlam 1968; Carlson et al. 1983; Lanicci and Warner 1991a). Surface moisture availability and topography, particularly the elevated terrain of the western CONUS and northern Mexico, act as fundamental controls on EML frequency and SCS environments (Lanicci et al. 1987; Benjamin and Carlson 1986; Benjamin 1986; Arritt et al. 1992; Li et al. 2021). Steep midlevel lapse rates associated with the EML often enhance convective available potential energy (CAPE), a necessary ingredient for convective storms, while the cap at the base of the EML can prevent or delay convective initiation (CI) over large areas, allowing additional diurnally driven increases in CAPE due to the absence of convective overturning (Agard and Emanuel 2017). As a result, any storms that do form have the potential to have more vigorous updrafts than if no EML or capping inversion were present (Carlson and Ludlam 1968; Carlson et al. 1983; Graziano and Carlson 1987).

Lanicci and Warner (1991a,b,c) performed the first comprehensive climatology of the EML. Using four years of observed

Denotes content that is immediately available upon publication as open access.

Corresponding author: Margo S. Andrews, mandrews4@niu.edu

Publisher's Note: This article was revised on 5 March 2024 to include the CC BY reuse license designation that was missing when originally published.

DOI: 10.1175/JCLI-D-23-0517.1

soundings over the central CONUS, they explored common EML synoptic patterns, relationships to SCSs, and spatiotemporal frequencies, firmly establishing that the EML is primarily a warm-season phenomenon most prevalent in the Great Plains. More recently, Ribeiro and Bosart (2018) examined EMLs in South America and compared them to their North American counterparts using the NCEP Climate Forecast System Reanalysis (CFSR; Saha et al. 2010). Ribeiro and Bosart (2018) confirmed and expanded upon prior work, finding the greatest frequency of EMLs in the southern Great Plains and Mexico during spring, with a northward-shifted, slightly reduced frequency maximum in summer, a result Li et al. (2020) were able to replicate using the European Centre for Medium-Range Weather Forecasts (ECMWF) fifth-generation atmospheric reanalysis (ERA5; Hersbach et al. 2020). While EML occurrence and spatiotemporal distribution are, therefore, fairly well understood, to the authors' knowledge, no research has examined the EML's inter- or intra-annual variability. In addition, potential trends in EML frequency and associated EML characteristics have not been researched to date.

Understanding the EML's variability and potential trends are important, as EMLs are often linked to high-impact convective weather even in regions well outside of the climatological maximum. In Minneapolis, for example, days with an EML have substantially more SCS reports than the calculated climatology (Cordeira et al. 2017). Likewise, in the Northeast, EMLs are present in a notable percentage of the severe thunderstorm environments that result in injuries and fatalities (Banacos and Ekster 2010). However, the presence of an EML is not a sufficient condition for SCSs (Cordeira et al. 2017).

The well-established ingredients required for SCSs are instability, moisture, vertical wind shear, and a lifting mechanism (e.g., McNulty 1985; Johns and Doswell 1992; Rasmussen and Blanchard 1998; Brooks et al. 2003). The existence of the warm, moist boundary layer air from the Gulf of Mexico and local moisture sources such as soils and vegetation, below the steep lapse rates of the EML, often ensures the presence of sufficient low-level moisture and can contribute to substantial instability (Molina and Allen 2019; Li et al. 2021; Tuckman et al. 2023; Zhang et al. 2023; Emanuel 2023). Combined with the vertical wind shear often present with the synoptic patterns favoring EML formation, it follows that EMLs are often supportive of SCSs (Carlson and Ludlam 1968; Carlson et al. 1983; Farrell and Carlson 1989; Lanicci and Warner 1991a,c; Banacos and Ekster 2010; Cordeira et al. 2017; Ribeiro and Bosart 2018), assuming there is adequate forcing for ascent in the form of vertical differential temperature advection, surface heating, orographically induced circulations, or surface convergence to overcome the inhibition (e.g., Carlson et al. 1983; McNulty 1995; Weckwerth and Parsons 2006; Cordeira et al. 2017). Springtime composites of SCS forecast parameters reveal that North American EML environments have higher CAPE, lower lifting condensation levels, and greater 0–1-km storm-relative helicity compared to South America, implying more favorable conditions for supercells and tornadoes if the stronger capping inversions in North America can be overcome (Ribeiro and Bosart 2018).

The presence of a considerable cap often prevents deep convection, with only 6%–8% (3%–6%) of favorable SCS environments in the eastern half of the CONUS (Great Plains) producing severe thunderstorms (Taszarek et al. 2020). Convective inhibition (CIN) provides an estimate of the strength of the capping inversion, measuring the negative buoyancy a parcel must overcome to reach the level of free convection. Since most storms form in unstable environments with less than 75–100 J kg^{-1} of absolute CIN, the magnitude of CIN provides some indication of the likelihood of CI (Bunkers et al. 2010; Gensini and Ashley 2011; Hoogewind et al. 2017; Taszarek et al. 2021a). Springtime composites in three CONUS regions reveal median absolute EML-related CIN of approximately 200 J kg^{-1} (Ribeiro and Bosart 2018). While absolute CIN above 200 J kg^{-1} is generally too strong to overcome, values between 50 and 200 J kg^{-1} can be beneficial to deep convective updrafts—permitting CAPE to increase with time and limiting storm coverage—provided that there is strong enough forcing to ascend and sustain updraft parcels through the capping inversion (Bunkers et al. 2010; Rasmussen et al. 2020). By examining the distribution of CIN associated with EMLs in all regions and seasons, we reveal the typical magnitude and seasonality of the cap and provide insight into how often EML environments may be favorable for deep convection. Furthermore, we investigate whether the significant spring and summer increases over the last four decades in CIN and midlevel lapse rates in the Great Plains (Taszarek et al. 2021a; Pilguj et al. 2022) are related to long-term changes in the frequency and/or characteristics of the EML. This was motivated by Taszarek et al. (2021a), who suggested that the increases in midlevel lapse rates and CIN were driven by significant trends toward hotter and drier boundary layers over the western CONUS, which should be increasingly favorable for the development of EMLs. Therefore, we calculate long-term trends in EML occurrence and relevant EML attributes, as more frequent EMLs and/or stronger capping inversions could have major implications for SCS frequency, intensity, and location in the future (Rasmussen et al. 2020; Taszarek et al. 2021a; Haberlie et al. 2022; Ashley et al. 2023).

Using an objective algorithm to automatically identify EMLs, we create an updated climatology of the EML in the CONUS and northern Mexico. The EML's typical frequency, spatial distribution, and spatial extent are calculated, as are EML attributes such as lapse rates, potential temperature, and CIN. The algorithm output is then examined to 1) compare to previous climatologies, 2) better understand the magnitude and distribution of the capping inversion at the base of the EML, and 3) determine whether the EML or its attributes exhibit substantial changes within the study period. Results provide insight into the variability and long-term trends of the EML.

2. Data and methods

a. Data

Data used in this research were generated using ERA5 over the 43-yr period from 1979 to 2021. ERA5 has a horizontal grid spacing of 31 km and 137 hybrid-sigma levels in the vertical, 28 of which are in the lowest two km (Hersbach et al. 2020; Copernicus Climate Change Service 2017). The superior vertical resolution of ERA5 compared to other existing

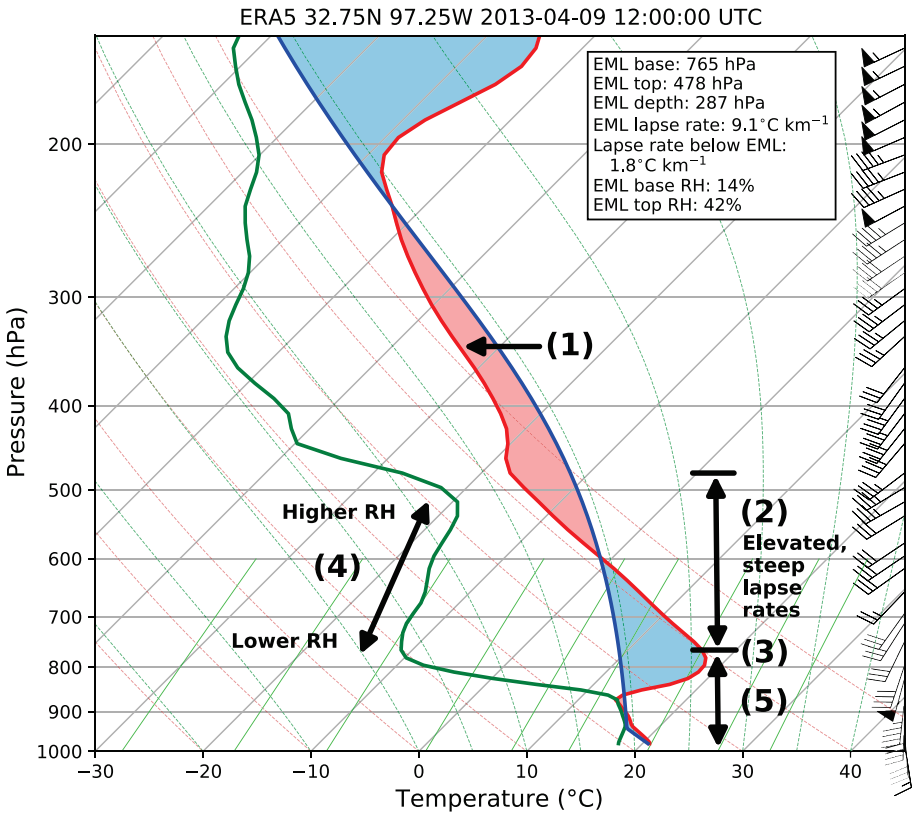

FIG. 1. Sample ERA5 vertical profile illustrating the required criteria for classification as an EML. Numbers and arrows correspond to the individual criteria: 1) greater than 0 J kg^{-1} of MUCAPE, 2) an environmental lapse rate of at least 8°C km^{-1} over a depth of at least 200 hPa, 3) an EML base above 1000 m AGL but below 500 hPa, 4) a higher RH at the top of the EML compared to the EML base, and 5) an average lapse rate below the EML base of less than 8°C km^{-1}. Bold horizontal lines near 2 and 3 denote the top and bottom of the EML.

reanalyses results in an improved depiction of the vertical temperature profile of the EML, including the capping inversion, which earlier reanalyses struggled to resolve (Brooks et al. 2003; Gensini et al. 2014a; Ribeiro and Bosart 2018; Taszarek et al. 2018; King and Kennedy 2019; Taszarek et al. 2021b). ERA5 does have biases, however, as it tends to underestimate CAPE, and, to a lesser degree, CIN, and has lower correlations compared to observed soundings in areas with sharp topographic changes (Taszarek et al. 2021b). Despite these limitations, reanalyses have proven to be an effective means to understand the climatology and long-term trends of SCSs and their environments (Brooks et al. 2003; Brooks 2009; Riemann-Campe et al. 2009; Gensini and Ashley 2011; Gensini and Brooks 2018; Gensini and Bravo de Guenni 2019; Tang et al. 2019; Taszarek et al. 2020; Li et al. 2020; Gensini 2021; Taszarek et al. 2021a; Pilguj et al. 2022). Various studies demonstrate that ERA5 is particularly well suited for climatological analysis of SCS environments due to its ability to capture these environments, and their synoptic-scale features, reasonably well (Li et al. 2020; Taszarek et al. 2021b; Pilguj et al. 2022). The 3-hourly ERA5 output is used (0000, 0300, 0600, 0900, 1200, 1500, 1800, 2100 UTC) over the study domain, focused roughly east of the continental divide (~107°W longitude) in the CONUS and northern Mexico, where the highest frequency of EMLs are found (Lanicci and Warner 1991a; Ribeiro and Bosart 2018; Li et al. 2020).

b. *EML identification algorithm*

In this study, an objective algorithm identifies EMLs using a modified version of the criteria presented by previous authors including Lanicci and Warner (1991a), Ribeiro and Bosart (2018), and Li et al. (2020). The algorithm is applied to vertical profiles of ERA5 temperature, pressure, specific humidity, and geopotential to locate grid points within the study period and domain that meet the following criteria (Fig. 1):

1) Greater than 0 J kg^{-1} of most unstable CAPE (MUCAPE),
2) An environmental lapse rate of at least 8°C km^{-1} over a depth of at least 200 hPa,
3) An EML base, defined as the first level of the layer with a lapse rate of at least 8°C km^{-1}, located at least 1000 m above ground level (AGL) but below 500 hPa,
4) A higher relative humidity (RH) at the top of the EML (defined as the last level of the layer with a lapse rate of at least 8°C km^{-1}) compared to the EML base, and
5) An average lapse rate below the EML base of less than 8°C km^{-1}.

The depth and lapse rate thresholds (criterion 2) are consistent with Li et al.'s (2020) selection following testing of various lapse rate and thickness combinations after determining that the frequency of the EML in ERA5 is highly sensitive to the depth and stability criteria used. These thresholds are more restrictive than Ribeiro and Bosart (2018) because, unlike the CFSR, ERA5 more accurately depicts both the magnitude and spatial distribution of midlevel lapse rates (Taszarek et al. 2021b). Criterion 3 is designed to eliminate the inclusion of steep lapse rates in the boundary layer and those that exist in the upper troposphere as the environmental lapse rate approaches the dry adiabatic lapse rate (Ribeiro and Bosart 2018). The final criterion further ensures that mixed layers originating at the surface are not identified as EMLs.

Though the algorithm is not capable of discerning the physical processes responsible for vertical profiles classified as EMLs, the MUCAPE requirement is included to eliminate some profiles that do not form via the downstream advection of a well-mixed boundary layer off of higher terrain. Both Lanicci and Warner (1991a) and Ribeiro and Bosart (2018) also use a minimum convective instability threshold. Similar to Ribeiro and Bosart (2018), the inclusion of the instability criterion eliminates a number of vertical profiles with subsidence inversions. Many of these profiles occur in the high terrain during the cool season and have zero MUCAPE, owing to cold and/or dry low-level air. The >0 J kg^{-1} threshold is less restrictive than other tested thresholds, while still eliminating many of the cases described above. The reduction in detected EML days due to this criterion occurs almost exclusively from November–April and varies greatly by location. Portions of the highest terrain in northern Montana, Colorado, and New Mexico have 32–48 fewer mean annual EML days, while the annual mean across most of the Great Plains is reduced by 8–24 EML days, with the largest reduction close to the high terrain. Though adding the instability requirement does substantially reduce the frequency of detected EMLs, it has the advantage of highlighting vertical profiles with convective potential.

The algorithm employing these five criteria is applied every 3 h to each grid point in the domain over the full 43-yr period. Grid points that meet all criteria are marked as having an EML at that time. Attributes of all EMLs, including EML thickness, base height, base pressure, lapse rate, mean potential temperature, maximum temperature, and CIN are also collected for further analysis.

c. EML occurrence and variability

To assess the EML's spatial distribution and seasonality, mean EML occurrence is computed in two ways. The average number of EML days is the primary metric of expected occurrence. Herein, an EML day is defined as a day (1200–1200 UTC) where an EML is present at a grid point for at least one of the 3-hourly time steps in the 24-h period. To permit a direct comparison to previous climatologies, the percentage of time steps with an EML present is also calculated (mean EML frequency).

EML days are then used to explore the variability of the EML. The maximum, minimum, and standard deviation are calculated annually and for each season at every grid point, revealing the upper and lower bounds of EML days at each location and the magnitude and regions of greatest interannual variability. To further analyze inter- and intra-annual variability, cumulative frequencies of EML days are calculated for each year in the study period at the grid point closest to eight city centers: Fort Stockton, TX; Lubbock, TX; Oklahoma City, OK; Garden City, KS; Colorado Springs, CO; Valentine, NE; Bismarck, ND; and Kansas City, MO. The cities selected provide a roughly even geographic distribution within the >10 mean EML days per year contour.

d. EML attributes

To explore the typical magnitudes of relevant EML characteristics, and how they vary with space and time, annual and seasonal composites of mean EML thickness, base height, base pressure, lapse rate, average potential temperature over the EML depth, and CIN are created using all time steps with an EML at each grid point. CIN is calculated with the virtual temperature correction (Doswell and Rasmussen 1994) using the lowest 100-hPa mixed-layer parcel (ML) and the most unstable parcel in the lowest 3-km AGL (MU). Seasonal box plots of the same variables at each aforementioned city contain all time steps with an EML, revealing the full distribution of these EML attributes within the study period. The seasonal distribution and interannual variability of EML area are examined using daily EML coverage. Daily EML coverage is calculated by multiplying the number of EML grid points in the study domain each day by the area of one grid box (961 km^2).

e. Long-term trends in the EML

To analyze trends in EML occurrence, EML days are first summed at every grid point for each year in the dataset. Trends are then calculated on the yearly values using the Theil–Sen estimator (Wilcox 2010). This method is frequently used in the atmospheric sciences (e.g., Gensini and Brooks 2018; Tang et al. 2019; Taszarek et al. 2021a; Pilguj et al. 2022) because it is nonparametric and relatively insensitive to outliers (Wilcox 2010). Trends in EML characteristics including lapse rates, maximum temperature, and CIN are calculated following the approach for EML days. The Theil–Sen estimator is applied to the annual means at each grid point, which are calculated using the 3-hourly values from time steps with an EML present. As with the EML day trends, the Theil–Sen slopes of EML attributes are normalized to show 10-yr changes, therefore denoting change per decade, and are tested for statistical significance using Kendall's τ statistic at the 95% significance level.

3. Results

a. EML occurrence and variability

Mean annual EML days are most frequent along and just east of the EML source regions in the western CONUS and

northern Mexico, with an average of 15–30 EML days per year over most of the Great Plains (Fig. 2a). Seasonally, peak EML occurrence is found in the spring (MAM), with the greatest number of EML days concentrated in the southern Great Plains and northeastern Mexico (12–21 EML days per year; Fig. 2c). This springtime maximum and its location are consistent with previous climatologies including Lanicci and Warner (1991a), Ribeiro and Bosart (2018), and Li et al. (2020). While the EML source region is primarily confined to northern Mexico in the early spring, it expands northward following solar zenith angle later in the warm season to include the high terrain of the western CONUS (Lanicci and Warner 1991a). The corridor of peak EML days follows, with a northward-shifted maximum of slightly lesser magnitude along the western extent of the central and northern Great Plains in the summer (JJA; Fig. 2d). EMLs east of the Mississippi River are rare, with one or fewer EML days per month. EMLs are also very rare in the winter (DJF) and fall (SON), owing to less intense surface heating and limited instability (Figs. 2b,e).

EML frequency (not shown) largely mirrors the spatial distribution and seasonal variability of EML days. The locations of the spring and summer maxima align with Ribeiro and Bosart (2018) and are quantitatively very similar to Li et al. (2020; cf. their Fig. 12) in these two seasons. Magnitudes of annual, winter, and fall EML frequency are less than that of Li et al. (2020) due to the addition of our minimum MUCAPE threshold. The difference is most notable in the winter when this criterion results in the removal of the greatest number of vertical profiles. Compared to Ribeiro and Bosart (2018), EML frequencies are less in all seasons, likely due to the sensitivity of EMLs to the chosen criteria, including the lapse rate and thickness thresholds (Li et al. 2020). Electing to use objective criteria of any threshold is a limitation because no one set of criteria is likely to detect all EMLs. It is possible that, for example, EMLs over certain regions are shallower or have lower lapse rates on average than those over the Great Plains. Regardless of the thresholds selected, some borderline cases may be excluded. In addition to the thickness and lapse rate thresholds, EML day results are also sensitive to the number of time steps used to define an EML day. Requiring two (three) time steps with an EML at a grid point in a 24-h period reduces the average number of EML days over much of the southern Great Plains and northeastern Mexico to 6–12 days (3–6 days) per spring season, although the annual and seasonal spatial distributions remain largely the same. Similarly, the expected number of EML days each summer over the high terrain of the northern and central Great Plains is reduced to 5–9 days (2–6 days), when two (three) time steps are used to define an EML day. Smoothing and/or biases in the reanalysis could create an additional source of error in select cases. Perhaps the most important aspect is that the algorithm be applied across all regions and intervals in a consistent manner as performed herein.

Although there is a well-established seasonal cycle for the EML, there is also substantial variability from year-to-year and season-to-season. Relatively large year-to-year variability is found in the Great Plains, where the standard deviation for annual EML days ranges from 4 to 10 days (Fig. 3c). Parts of southwest Texas and northwestern Oklahoma experience the greatest range in annual EML days within the 1979–2021 period, with as many as 50–56 and as few as 9–15 EML days in a year (Figs. 3a,b). On a seasonal basis, the range between the period maximum and period minimum is as high as 39 EML days in spring in southern Texas and northeastern Mexico (Figs. 3g,h) and 24–32 EML days in the western portion of the central and northern Great Plains in summer (Figs. 3j,k).

Intra-annual variability differs by location. Most EML days in the southern Great Plains occur before July, after which variability noticeably increases (Figs. 4a–d). This is true of Fort Stockton, Lubbock, Oklahoma City, and Garden City, which see a relatively small spread in year-to-year cumulative EML days from January to June, followed by increased variability. Increased variability after June may be a function of a few factors, all of which make it more difficult to consistently organize EMLs. In the summer, this is likely a northward displaced polar jet steam (with lack of EML advection) and a less focused EML source region compared to spring, whereas in the fall and winter, less intense surface heating and convective instability are likely the major limiting factors. Further north in Valentine and Bismarck, EML days increase relatively linearly from April through October (Figs. 4f,g). The steady increase in EMLs and fairly constant variability in the northern Great Plains likely reflects this region's range of EML source regions as compared to a more spatially and temporally focused source in the southern Great Plains during spring. Although EML occurrence and intra-annual variability differ by location, the year with the maximum number of EML days at all eight cities is 2011 or later (Figs. 4a–h).

The diurnal distribution of EMLs across the study domain differs throughout the year. In spring and summer, EMLs are most frequent from 0600 to 1500 UTC and least common from 2100 to 0000 UTC (Figs. 5a,b). Fewer EMLs in the afternoon and early evening are the result of a couple of factors. In some cases, storms initiate and erode the EML locally in the afternoon and/or evening. In other instances, typical afternoon surface-based heating results in steep low-level lapse rates, such that the algorithm's fifth criterion, requiring lapse rates below the EML base of $<8°C\ km^{-1}$, is not satisfied if the steep lapse rates continue above the PBL without a break (i.e., no capping inversion present). In contrast to spring and summer, winter and fall see very minor differences in the number of EMLs throughout the day (not shown).

b. *EML attributes*

Most EML attributes vary seasonally, including EML area. When all days in the study period with at least one EML grid point are considered, spring has the largest daily mean and median EML coverage, followed by summer (Fig. 6a). Daily EML area in the spring averages just over 415 000 km^2, with a median area of approximately 230 000 km^2, slightly larger than the state of Minnesota (Fig. 6a). In the summer, the mean and median daily EML area are about 307 000 and 178 000 km^2, respectively (Fig. 6a). These measures of central tendency indicate that while some EMLs are expansive, EMLs cover only a small portion of the study domain on most

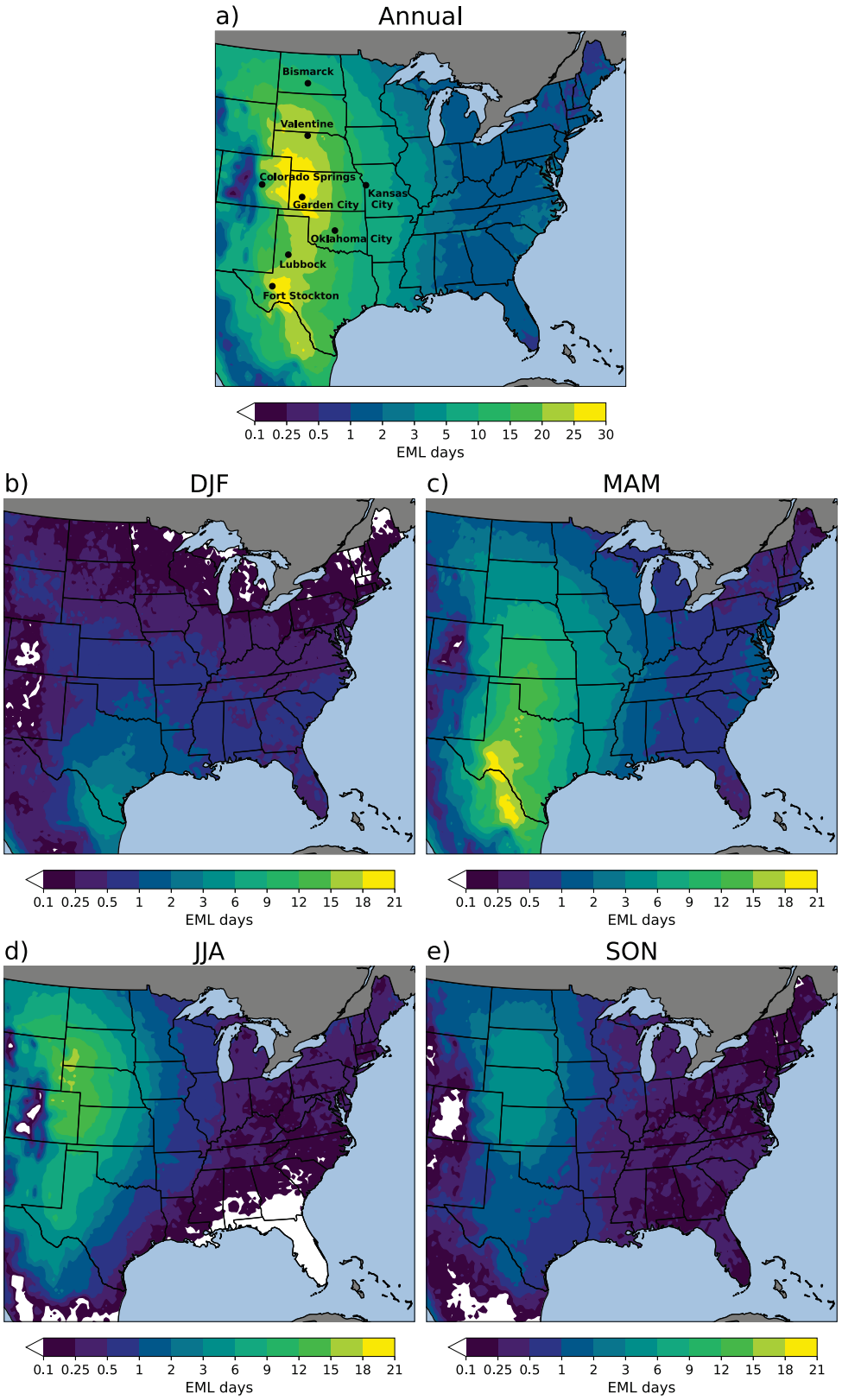

FIG. 2. Mean EML days (a) annually, and by season for (b) winter, (c) spring, (d) summer, and (e) fall. An EML day is defined as a day (starting at 1200 UTC) where an EML is present at a grid point for at least 1 h. The locations of the eight cities discussed in Figs. 4 and 8 are labeled in (a).

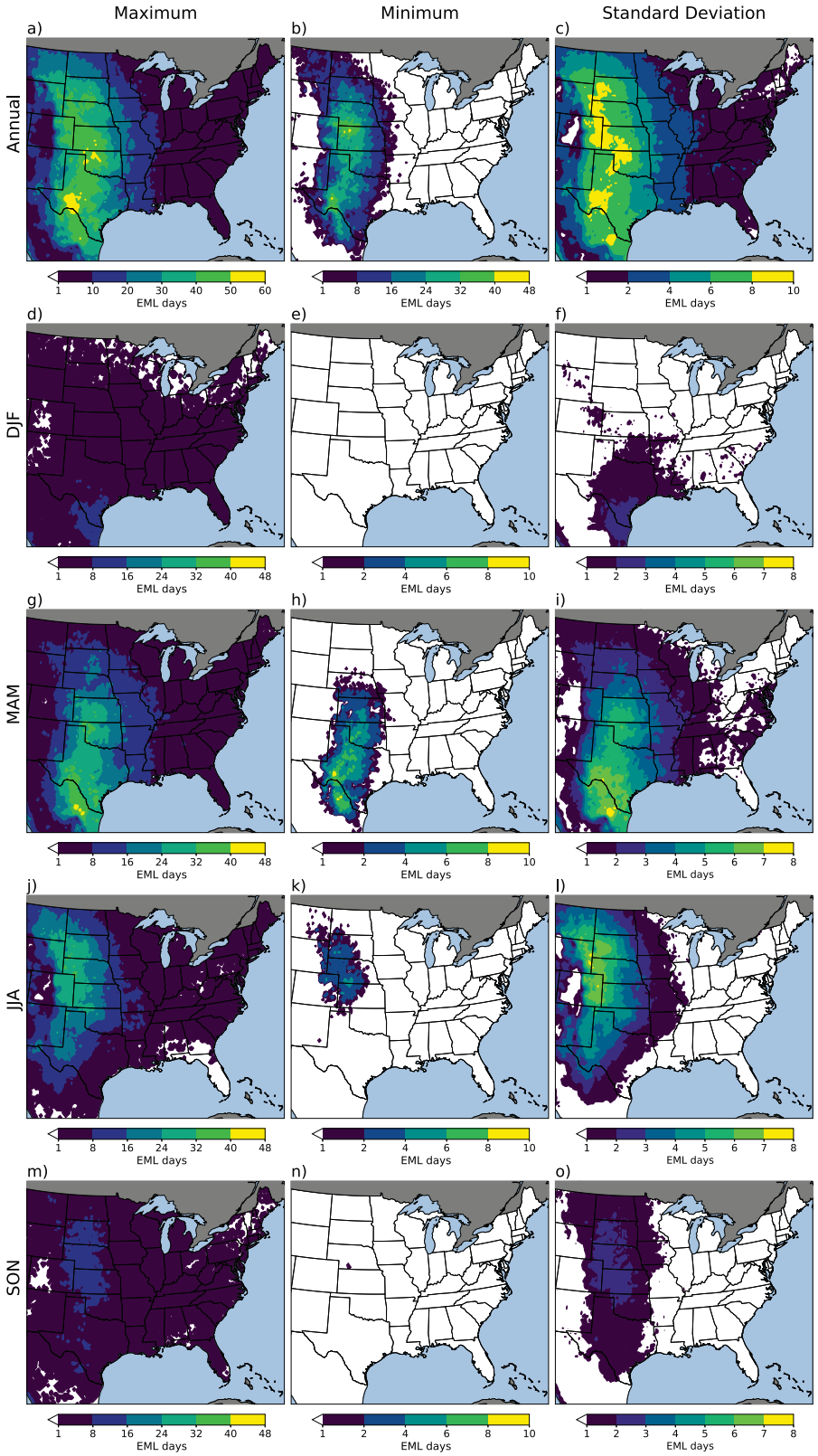

FIG. 3. (a),(d),(g),(j),(m) Maximum; (b),(e),(h),(k),(n) minimum; and (c),(f),(i),(l),(o) standard deviation of EML days (a)–(c) annually and in (d)–(f) winter, (g)–(i) spring, (j)–(l) summer, and (m)–(o) fall.

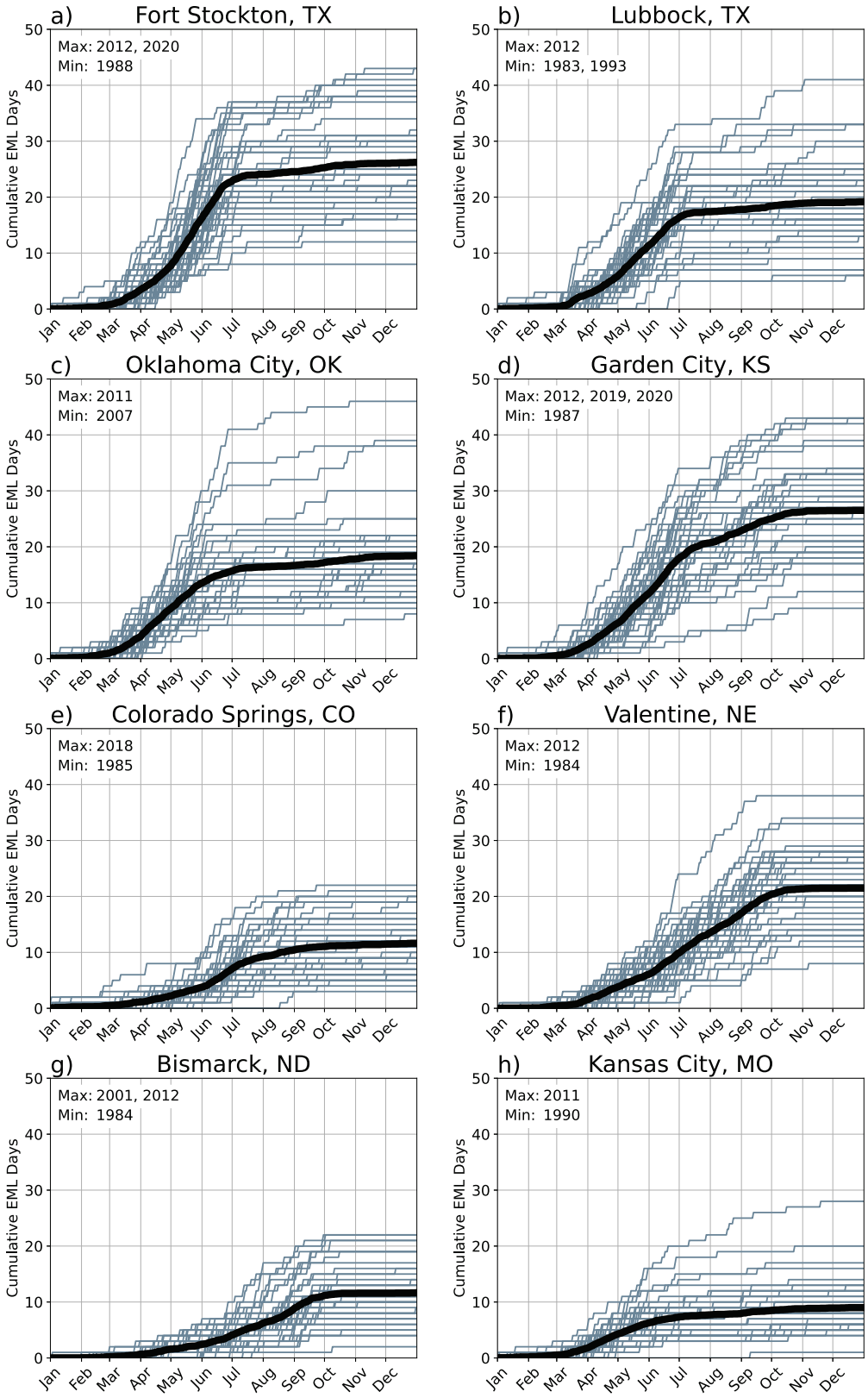

FIG. 4. Annual cumulative sums of EML days at eight select U.S. cities. Cumulative sums for each year are shown in gray. Thick black lines denote the 1979–2021 means. The year with the maximum and minimum cumulative EML days from 1979 to 2021 is indicated for each city.

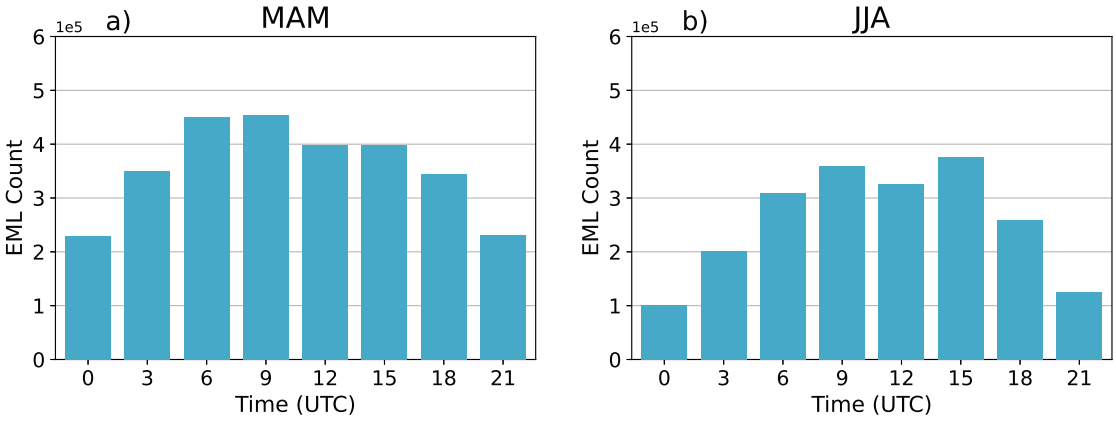

FIG. 5. Cumulative number of vertical profiles classified as EMLs by hour of the day for (a) spring and (b) summer.

days. Although winter and fall have relatively limited EML coverage, there is a substantial range in daily EML area in all seasons, with 3018 days in the period (19%) with zero EML grid points within the domain, and 77 days (0.5%) with EML coverage exceeding 2 million km^2.

In addition to seasonal differences, there is also sizable interannual variability in EML area. Median daily EML area in spring ranges from approximately 114 000 km^2 in 1992 to 574 000 km^2 in 2012, whereas summer has an interannual range of nearly 348 000 km^2 between 1984 and 2011 (Fig. 6b). In terms of cumulative EML area, spring has the greatest year-to-year range (47 million km^2), followed by summer (40 million km^2; Fig. 6c). Once again, this variability emphasizes that individual years can deviate substantially from the climatological mean and median. EML area can also differ greatly from one year or season to the next, likely due to the

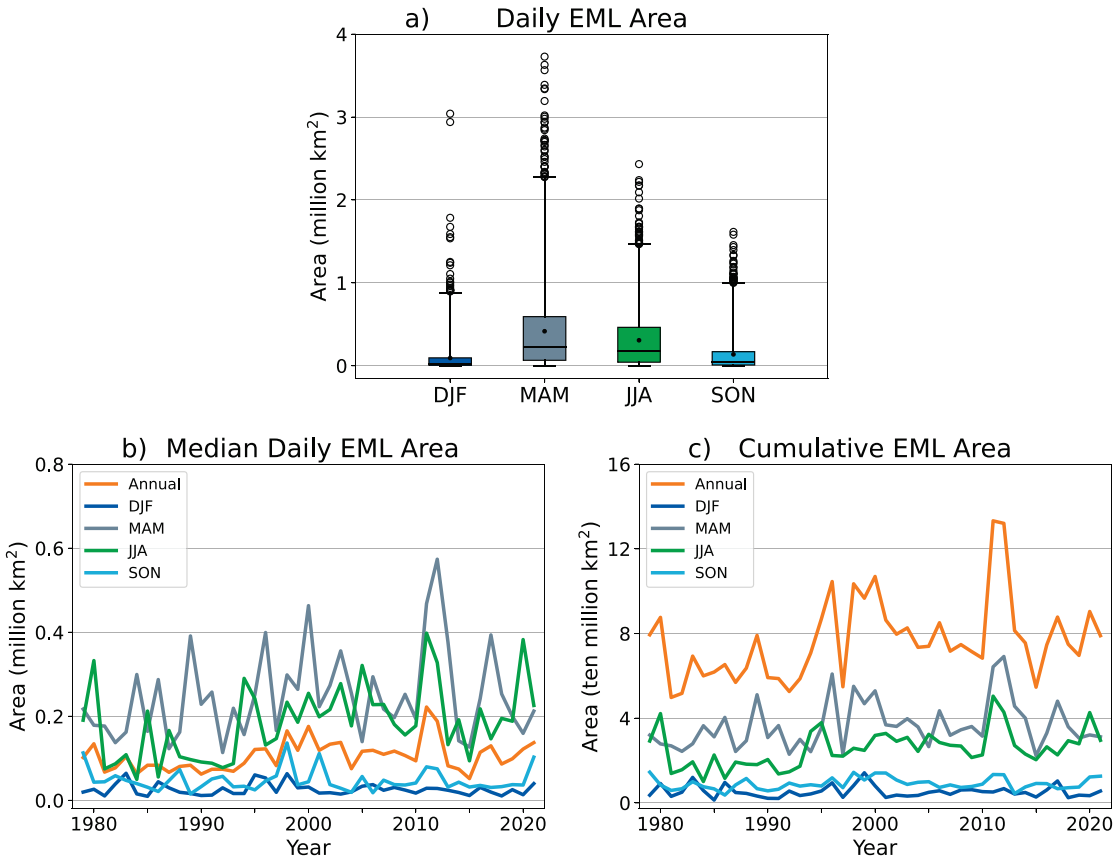

FIG. 6. (a) Daily EML area, (b) median daily EML area, and (c) cumulative EML area for days with an EML in winter, spring, summer, and fall. Boxes in (a) indicate the interquartile range, while dots and lines within the boxes denote the mean and median, respectively. Whiskers indicate the 1st and 99th percentiles and circles represent outliers.

sizable interannual variability in the aridity of EML source regions such as the southwest CONUS and northern Mexico (Seager et al. 2018). One notable example of interannual variability is the increase in EML area between 2010 and 2011, most evident annually and in the warm season (Figs. 6b,c). The relative maxima in EML area in 2011 and 2012 may be related to the significant La Niña and drought conditions in the southwestern CONUS at the time (NOAA 2023).

EML base pressure and base height also vary throughout the year. In the spring across the Great Plains, mean EML base height and base pressure are 2000–2500 m AGL and 700–750 hPa, respectively (Figs. 7c,h), consistent with Ribeiro and Bosart's (2018) climatology. Compared to spring, EML bases in summer and fall are, on average, found at higher pressures (750–800 hPa) and lower AGL heights (1500–2000 m AGL) over much of the Great Plains and parts of the Midwest (Figs. 7d,e,i,j). This result is counterintuitive. Warmer temperatures in the summer suggest deeper PBLs, implying EML bases should instead rise from spring to summer. However, Lanicci and Warner (1991a) noted the same decrease throughout the warm season and determined it was due to the more frequent occurrence of synoptic patterns favoring subsidence in the late spring and summer. In all seasons, EML base heights increase with eastward extent across the domain, while mean base pressures decrease. This eastward increase in EML base height in the Great Plains is physically reasonable because the surface elevation decreases eastward from the Rocky Mountains. However, east of the Mississippi River there are relatively few EMLs, meaning average EML attributes in this region, particularly in the winter and fall, should be interpreted with caution.

EML depth is largely consistent across space and time, with mean depths of 225–250 hPa at nearly all locations in all seasons (Figs. 7l–o and 8a). The exceptions, such as Valentine in winter and Fort Stockton in fall, generally have very few EMLs in their respective seasons. Although the means are generally consistent, likely due in part to the relatively strict EML depth criterion (≥200 hPa) within the EML detection algorithm, there is still a sizable spread in EML depth, with thicknesses that exceed 300 and even 350 hPa in all seasons (Fig. 8a).

An east-to-west-oriented potential temperature gradient is present between the Rockies and the Great Plains annually, with the highest mean EML potential temperatures along and just east of the mountains, close to the EML source regions (Fig. 9a). In the winter, spring, and fall, average EML potential temperature generally increases from north to south (Figs. 9b,c,e), with springtime values that range from 306 K near the U.S.–Canadian border to 322 K over parts of Mexico. A function of the range of EML source region temperatures, this north-south gradient was also found in spring by Lanicci and Warner (1991a). Due to the decreased meridional temperature gradient in the summer, there is very little variation in mean EML potential temperature across the domain (Fig. 9d). Summer also has the highest mean EML potential temperatures, with values of 318–320 K at all locations except for the far northern CONUS (Figs. 9d and 8b). Mean warm season values in the Great Plains are similar to Ribeiro and Bosart's (2018) range of 316–320 K.

Annually, the steepest mean EML lapse rates (8.9°–9.0°C km^{-1}; Fig. 9f) are located close to the high terrain of the Rocky Mountains with decreasing values to the east, similar to various climatologies of 700–500-hPa lapse rates in the CONUS (e.g., Brooks et al. 2003; Taszarek et al. 2021b). The orientation of the steepest lapse rates in spring are consistent with a primary source region of northern Mexico (Fig. 9h). From spring to fall, the steepest mean lapse rates (8.8°–9.1°C km^{-1}; Figs. 9h–j) expand northward with time, following maximum EML frequency. This northward expansion from spring to summer is consistent with a much broader source region extending into the high terrain of the western CONUS later in the warm season (Lanicci and Warner 1991a) and aligns well with Ribeiro and Bosart (2018; cf. their Fig. 5). Quantitatively, the magnitude of the steepest lapse rates in spring and summer are approximately 0.8°C km^{-1} larger than Ribeiro and Bosart's (2018) values. This difference may be related to the much higher vertical resolution of ERA5 compared to CFSR. Ribeiro and Bosart (2018) noted that CFSR EML lapse rates were an average of 0.7°C km^{-1} less than lapse rates calculated from observed soundings, in part due to limited vertical levels. While this study did not perform a comprehensive comparison of ERA5 and observed EML soundings, Taszarek et al. (2021b) found a correlation of 0.94 between the midlevel lapse rates of the two datasets, providing confidence in ERA5's ability to represent EML lapse rates reasonably well.

Seasonally, the highest mean absolute MLCIN (375–450 J kg^{-1}) associated with EMLs is confined to far southern Texas and northern Mexico in the winter and spring (Figs. 9l,m), the same areas where EML days are maximized (Figs. 2b,c). The magnitude of the capping decreases with northward extent in both seasons, with a mean of 225–375 J kg^{-1} of absolute EML MLCIN in spring over the remaining portions of the southern and central Great Plains (Fig. 9m). This northward decrease in the strength of the cap was anticipated because the magnitude of the cap is partially a function of the surface temperatures in the EML source regions. As a result, the warmer source regions further south in the winter and spring typically have warmer EML bases and larger inhibition. Although Ribeiro and Bosart (2018) used a different methodology to look at CIN associated with EMLs, they also found mean absolute values in spring of greater than 200 J kg^{-1} over the Great Plains and Mississippi Valley. From spring to summer, the region of greatest inhibition shifts northward and expands, with mean absolute values of 300–375 J kg^{-1} of MLCIN over the majority of the Great Plains (Fig. 9n). The warm season means in the Great Plains are well above the threshold (absolute CIN of 75–100 J kg^{-1}) under which most convective storms in favorable environments form (Bunkers et al. 2010; Gensini and Ashley 2011; Hoogewind et al. 2017; Taszarek et al. 2021a). Additionally, absolute CIN above 200 J kg^{-1} is generally considered prohibitive (Rasmussen et al. 2020), meaning that a substantial number of EML environments are not supportive of convection, even if all other ingredients are favorable. Domain-wide, approximately 58% and 68% of EMLs in spring and summer, respectively, have absolute MLCIN values above 200 J kg^{-1}. The spatial distribution and magnitude of EML-

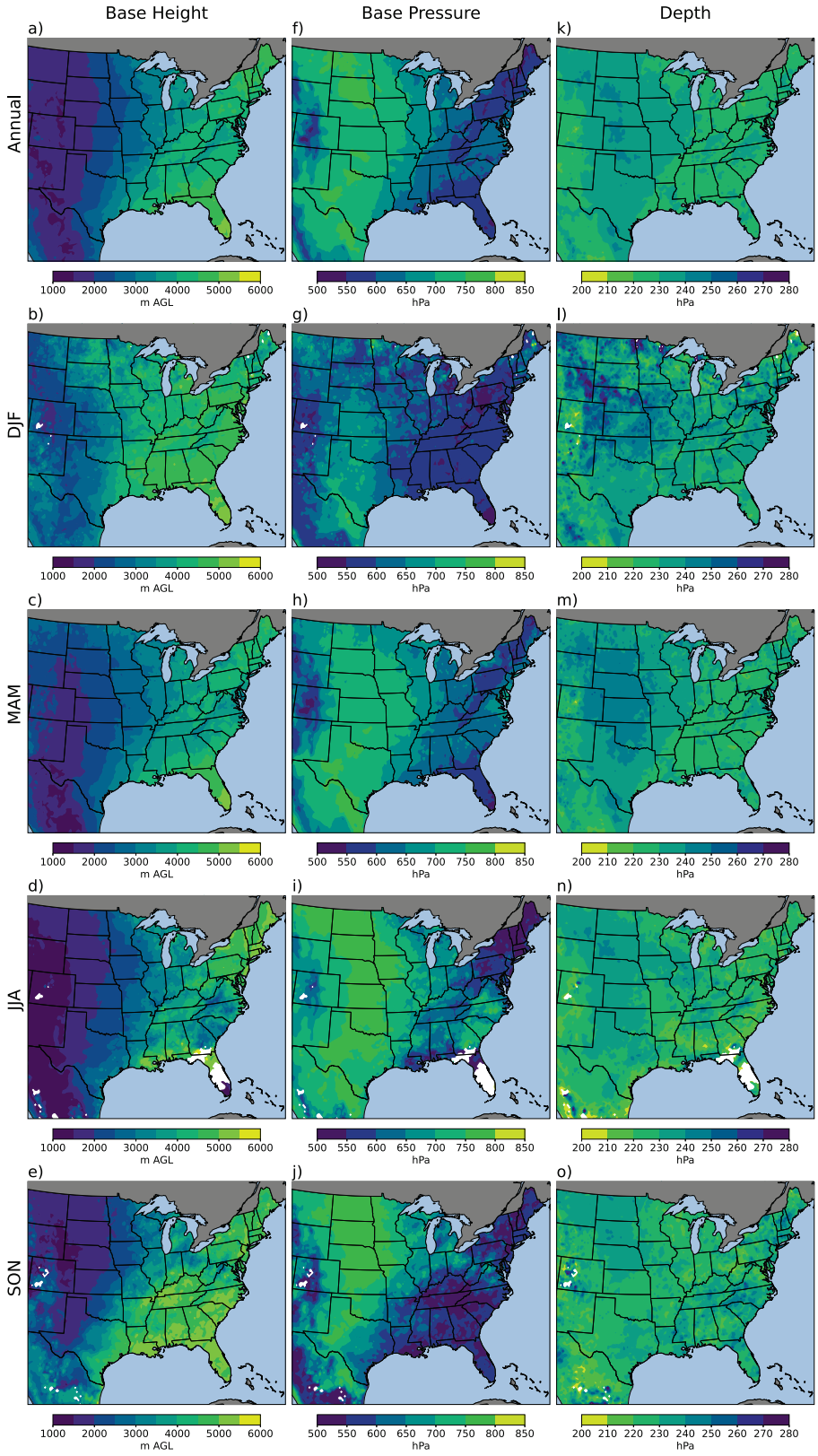

FIG. 7. (a)–(e) Mean EML base height, (f)–(j) mean EML base pressure, and (k)–(o) mean EML depth (a),(f),(k) annually and in (b),(g),(l) winter; (c),(h),(m) spring; (d),(i),(n) summer; and (e),(j),(o) fall.

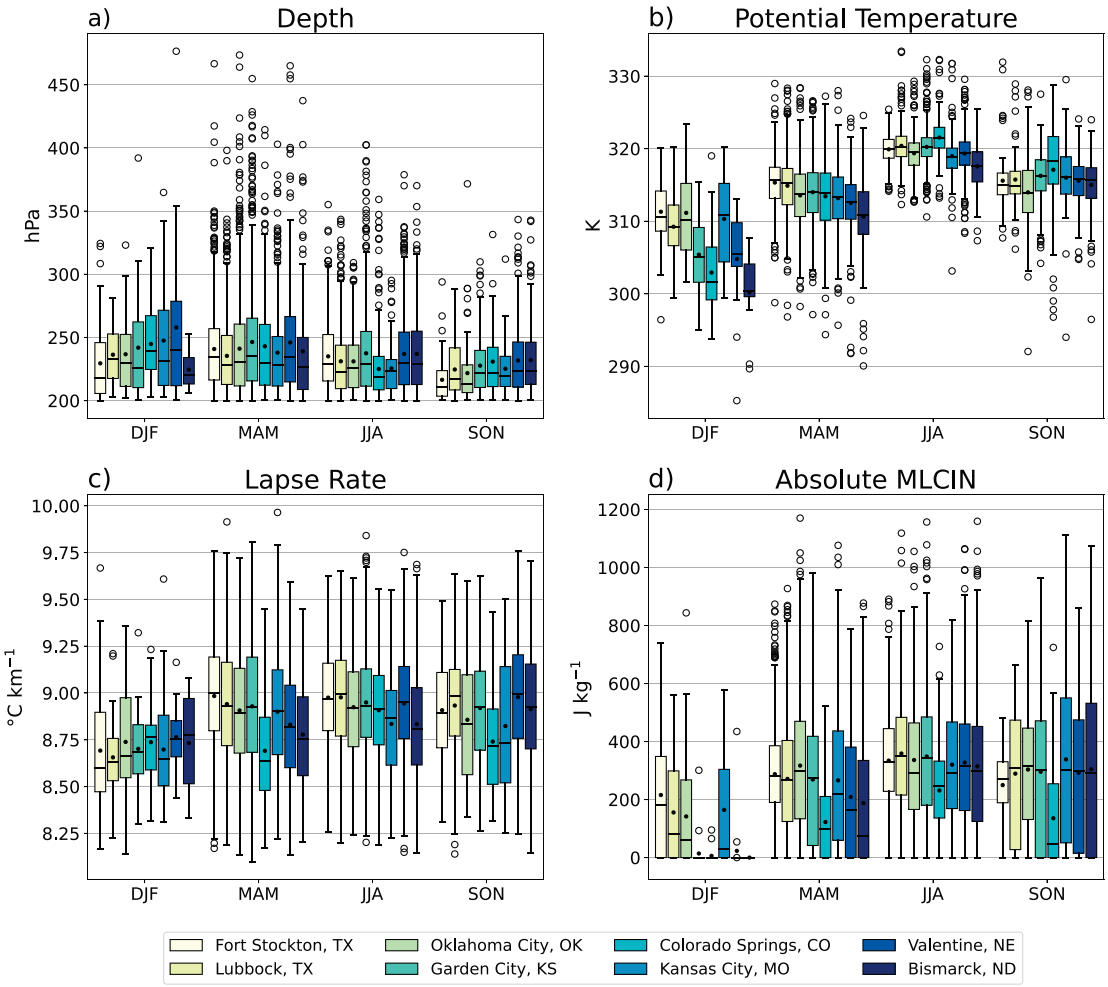

FIG. 8. Boxplots of seasonal (a) EML depth, (b) mean EML potential temperature, (c) EML lapse rate, and (d) absolute EML MLCIN at eight select U.S. cities. Boxes indicate the interquartile range. Dots and lines within the boxes denote the mean and median, respectively. Whiskers indicate 1.5 times the interquartile range and circles represent outliers.

related absolute MUCIN (not shown) closely resemble that of MLCIN in all seasons.

Despite large mean inhibition, there are plenty of instances where EMLs may be supportive of deep convection, including SCSs. For example, while all cities have prohibitive mean and median absolute EML MLCIN in at least one season, they also have a sizable number of EMLs with moderate and even weak inhibition (Fig. 8d). Deep convection is often found near the periphery of an EML—sometimes referred to as an "underrunning" scenario—where CIN is typically weaker compared to the EML center (Carlson and Ludlam 1968; Carlson et al. 1983; Keyser and Carlson 1984; Lanicci and Warner 1991b; Ribeiro and Bosart 2018).

c. *Long-term trends in the EML*

Statistically significant increases in EML days are found annually and in all four seasons (Fig. 10). On an annual basis, increases are concentrated in the High Plains, extending from Montana and western North Dakota to northern Mexico (Fig. 10a). The most notable trend in annual EML days occurs from northern Nebraska to southwest Texas, with increases on the order of 4–5 more EML days per decade. Spring and summer (Figs. 10c,d) are largely responsible for the annual trend, with significant springtime increases of 1.5–3 EML days per decade in northern Mexico and western Texas, Oklahoma, and Kansas (Fig. 10c). In the summer, the largest changes are located further north, with 2–4.5 more EML days per decade over the high terrain of the central and northern Great Plains (Fig. 10d). These warm season increases in EML days are likely responsible for the differential warming with height noted in observations and ERA5 from 1980 to 2018 (Pilguj et al. 2022). Maximized in the spring and summer between 2 and 3 km AGL over the Great Plains (Pilguj et al. 2022), the significant warming trend is consistent with the typical height of the EML base in these seasons (Figs. 7c,d), and the more frequent appearance of the EML over this region with time (Figs. 10c,d).

The upward trend in EML days is likely driven by warming and drying in the western CONUS during the study period. Increasing near-surface temperatures in the western and

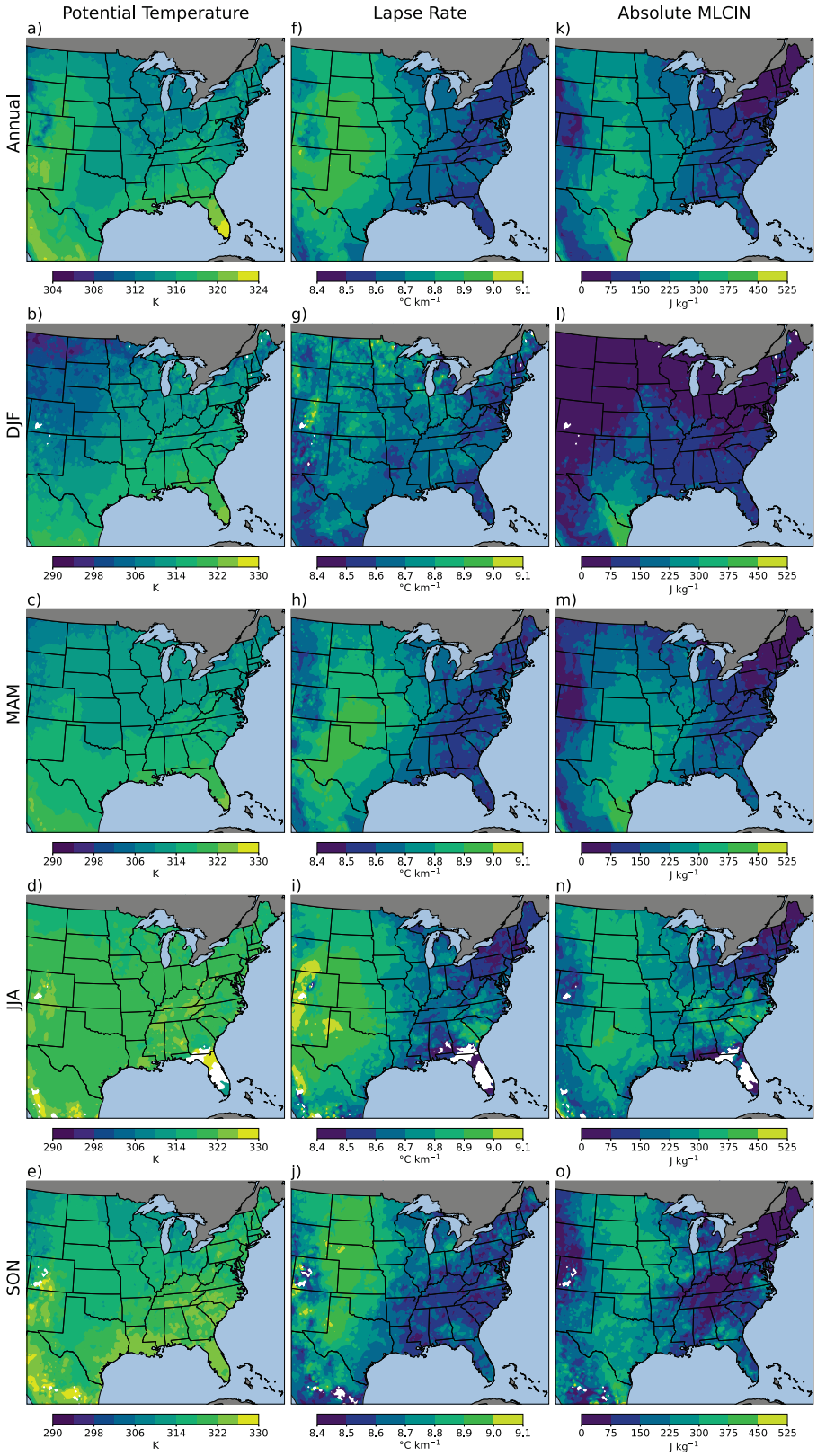

FIG. 9. (a)–(e) Mean EML potential temperature, (f)–(j) mean EML lapse rate, and (k)–(o) mean absolute EML MLCIN (a),(f),(k) annually and in (b),(g),(l) winter; (c),(h),(m) spring; (d),(i),(n) summer; and (e),(j),(o) fall.

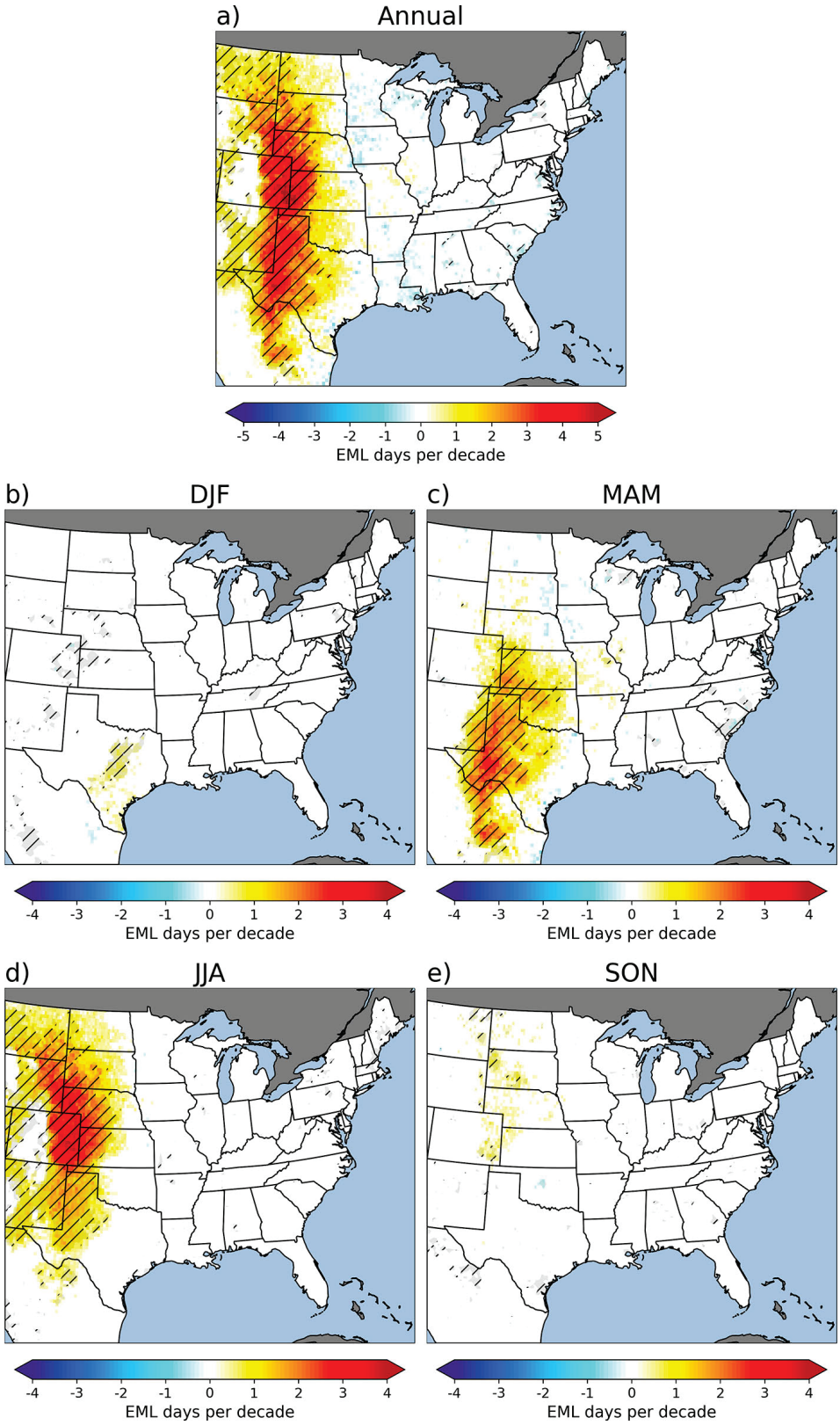

FIG. 10. Theil–Sen slope of the yearly gridpoint sum of EML days normalized per decade (a) annually and by season in (b) winter, (c) spring, (d) summer, and (e) fall. Hatching indicates statistical significance (p value ≤ 0.05) using Kendall's τ statistic.

southwestern CONUS during this time are well documented by both observations and reanalysis, with observed increases between 0.1° and 0.5°C decade^{-1} (IPCC 2022) and statistically significant increases in the 95th percentile of ERA5 2-m temperatures (Taszarek et al. 2021a). Likewise, drying trends in the western CONUS are observed via decreases in 0–500-m mixing ratio and 0–4-km relative humidity in observations and ERA5 (Taszarek et al. 2021a; Pilguj et al. 2022). Warming surface temperatures and steepening low-level (0–3-km) lapse rates in the EML source regions of both datasets (Taszarek et al. 2021a; Pilguj et al. 2022) strongly suggest that the warming and drying in the west contributed to the increase in EML days by increasing the maximum EML temperature and steepening EML lapse rates.

Since the EML is defined as a continuous layer of steep lapse rates, the maximum EML temperature is located at the EML base. The temperature at the EML base is a direct reflection of the surface temperatures in the western CONUS, since the PBL is advected downstream during EML formation. Due to the low-level warming and drying trends in the western CONUS, statistically significant trends in maximum EML temperature are found annually and in spring and summer (Figs. 11a–c). In spring, significant increases in maximum EML temperature are concentrated in the western portions of the central and southern Great Plains (1–2 K decade^{-1}), with a secondary area of warming centered over eastern Kansas and western Missouri (1.5–2.5 K decade^{-1}; Fig. 11b). Summertime increases in EML base temperature extend further north, from eastern Colorado through Montana (0.5 K decade^{-1}; Fig. 11c).

Annually, the western corridor of increasing EML base temperatures (Fig. 11a) matches well with the increases in EML days (Fig. 10a). This agreement was anticipated because warmer EML bases should support steeper EML lapse rates, thereby increasing the number of EMLs, since EMLs are defined in part as having lapse rates of a certain magnitude. Spatially, the locations of statistically significant trends in maximum EML temperature and mean EML lapse rates are also very similar, further supporting the notion that the increase in EML days is driven by the steepening of lapse rates by warmer near-surface temperatures in EML source regions. Like maximum EML temperatures, mean EML lapse rates increase in the western Great Plains (0.02°–0.1°C km^{-1} decade^{-1}), with secondary areas of increases over eastern Kansas and western Missouri (Fig. 11d). Although small in magnitude, the largest increases in spring and summer are found in the central Great Plains (Figs. 11e,f). East of the Rockies, the annual increases (Fig. 11d) are similar in magnitude and location to the increases in the 95th percentile of midlevel lapse rates in ERA5 over approximately the same period (Taszarek et al. 2021a).

In addition to supporting steeper lapse rates, warmer EML base temperatures also support a more strongly capped environment below the EML base, evident by the significant increases in absolute EML MLCIN (Figs. 11g–i) collocated with increases in maximum EML temperature (Figs. 11a–c). Annually, the absolute MLCIN associated with EMLs increases 15–40 J kg^{-1} each decade over most of the western Great Plains (Fig. 11g). Seasonally, the most substantial and widespread increases in EML-related capping occur in the spring over the southern half of the Great Plains (20–40 J kg^{-1} decade^{-1}; Fig. 11h). In the summer, the largest increases in absolute MLCIN are concentrated over eastern Montana (Fig. 11i). Increases in absolute MUCIN associated with EMLs (not shown) are nearly identical to MLCIN trends in all seasons. Increased EML capping could have major implications for the spatial distribution and frequency of the SCS climatology in the CONUS, some of which may already be occurring (e.g., Gensini and Brooks 2018; Gensini et al. 2020), and are projected to occur (Haberlie et al. 2022; Ashley et al. 2023). Increasing inhibition could prevent convection entirely, or delay the timing of CI, in some cases enhancing the likelihood of stronger storms through the increase of instability with diurnal heating (e.g., Bunkers et al. 2010; Rasmussen et al. 2020). The trend toward more absolute CIN is consistent with previous work finding significant increases in inhibition over the Great Plains in observations and ERA5 over the last four decades in spring and summer (Taszarek et al. 2021a; Pilguj et al. 2022). While these studies do not isolate EML-related CIN, the increases in stability are more than likely influenced by warmer EML bases and more frequent EMLs.

Spatially, regions with more EML-related inhibition (Figs. 11g–i) are similar to those with more EML days (Figs. 10a,c,d), implying that the stronger capping is directly linked to the warmer EML base temperatures and steeper lapse rates supporting the increase in EML frequency. Increases in EML days and warmer EML base temperatures may help explain the rise in environments inhibiting CI (absolute CIN $>$ 75 J kg^{-1}) and the decrease in the number of favorable environments producing precipitation over the Great Plains from 1979 to 2019 (Taszarek et al. 2021a). If the warming and drying trends in the western CONUS continue to drive an increase in PBL lapse rates that are subsequently advected downstream, steeper midlevel lapse rates will likely continue to cause an increase in EML frequency. In addition, warmer temperatures at the base of this advected layer will continue to increase the magnitude of CIN, particularly across the Great Plains. Relevant SCS climate change simulations suggest that this increase in inhibition will persist in the CONUS (Gensini et al. 2014b; Gensini and Mote 2015; Hoogewind et al. 2017; Rasmussen et al. 2020; Haberlie et al. 2022; Ashley et al. 2023), which could be in part due to a continuing trend toward more EMLs in a future climate. However, the latter half of the 1979–2021 period experienced a particularly noteworthy drought in the western and southwestern CONUS, as indicated by the Palmer Drought Severity Index (NOAA 2023). While it is likely that the warming and drying trends will continue to persist due to climate change, it is also possible that any future years with wetter conditions in the western CONUS may somewhat mitigate the increasing trend in EMLs and EML-related CIN, at least in the short term.

4. Discussion and conclusions

This study sought to create an updated high-resolution climatology of the EML to analyze variability and changes in EML occurrence and characteristics over the last four

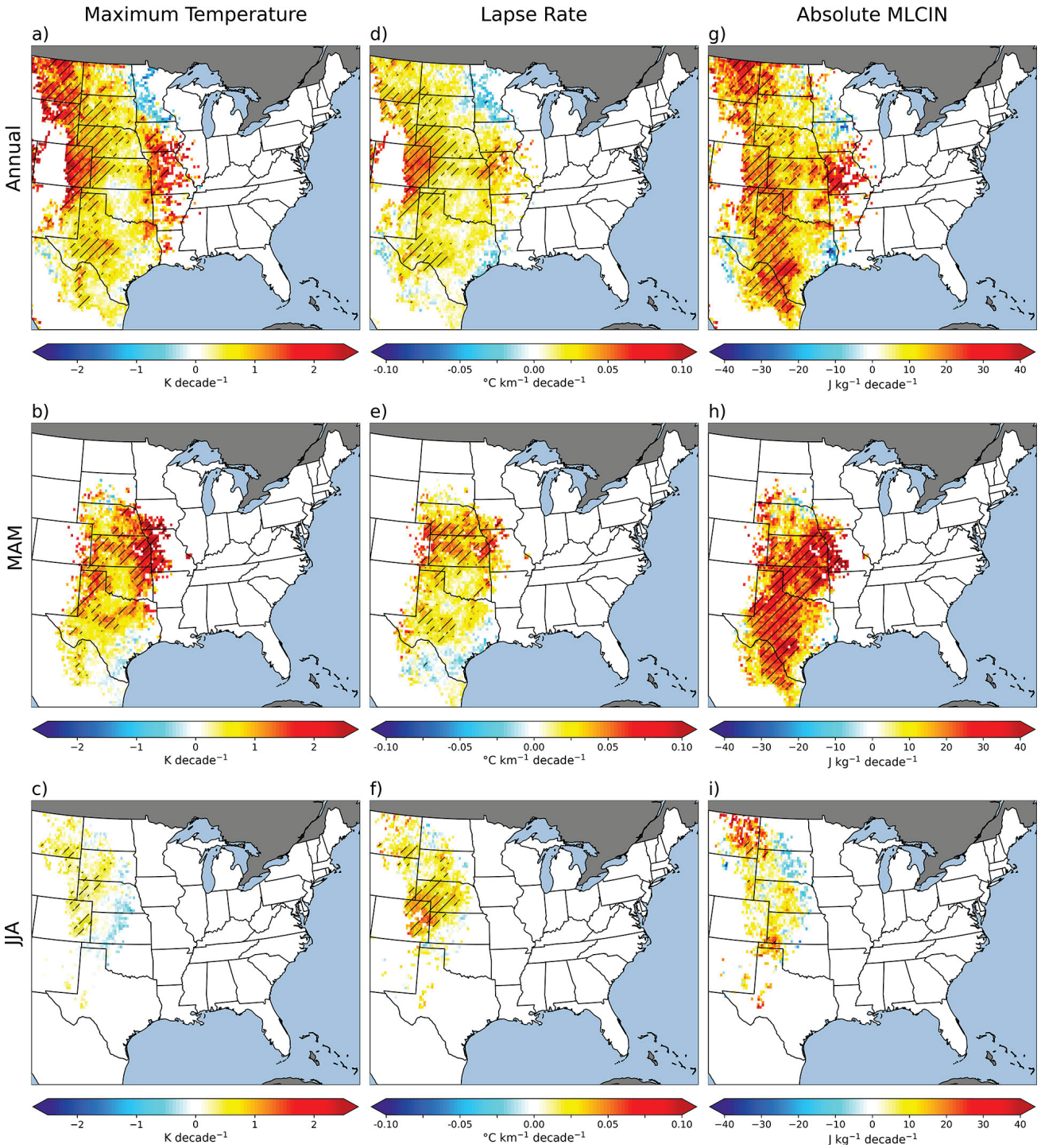

FIG. 11. Theil–Sen slope of mean yearly (a)–(c) EML maximum temperature, (d)–(f) EML lapse rate, and (g)–(i) absolute EML MLCIN normalized per decade. (top) The annual trends, (middle) the spring trends, and (bottom) the summer trends. Hatching indicates statistical significance (p value ≤ 0.05) using Kendall's τ statistic.

decades. EML days were maximized in the spring, with the highest frequency concentrated over the southern Great Plains and northeastern Mexico (mean of 12–21 days yr^{-1}). Following the poleward expansion of the EML source region from spring to summer, the peak shifted northward to the high terrain of the central and northern Great Plains (mean of 10–18 days yr^{-1}). EML days were relatively rare outside of the Great Plains, owing to the increased distance from source regions, while limited surface heating and instability resulted in very few EML days in the winter and fall. EML frequency generally aligned well with previous studies, with the most notable differences a result of the criteria used to define the air

mass. While no set of criteria can capture all EMLs, the similarities among results (despite different datasets), combined with ERA5's superior vertical resolution compared to previous reanalyses, provided confidence in the ability of the selected criteria to produce reasonably accurate and meaningful results.

Despite well-established normals, substantial interannual variability was found, with a difference of 15–40 EML days between the period maximum and minimum in spring throughout the southern and central Great Plains. Variability of this magnitude may have influenced severe storm frequency since EMLs can both suppress and enhance convection (e.g., Carlson and Ludlam 1968; Carlson et al. 1983; Graziano and Carlson 1987). Future work could determine whether years with a particularly high or low number of EML days were correlated with more or less severe storm reports compared to climatology.

EMLs were most frequent overnight through midmorning in the spring and summer, with far fewer EML occurrences at 2100 and 0000 UTC, often due to the erosion of portions of the EML by convection. Daily EML coverage over the domain was largest in the spring, although there was substantial spread and interannual variability in all seasons. All additional EML variables except EML depth exhibited notable seasonal variability. The steepest mean EML lapse rates were located in the Great Plains and expanded northward from spring to fall. Mean EML potential temperature decreased with northward extent in all seasons except for summer, which had the least variable and highest mean values across the domain. Finally, the average MLCIN associated with EMLs in all seasons indicated that a sizable proportion of EMLs were prohibitive (absolute MLCIN > 200 J kg^{-1}) for convection, although there were many other EMLs with capping inversions that may have been more easily overcome through forcing.

The most notable trends in EML days were found in the regions where EMLs were most frequent, with statistically significant increases in the southern Great Plains in spring and the western portions of the central and northern Great Plains in summer. These seasonal trends drove significant increases on the order of 4–5 more EML days per decade throughout the High Plains. More frequent EML occurrence is aligned with previous findings noting increased warming between 2 and 3 km AGL and significant increases in absolute CIN over the same period and region in the warm season (Taszarek et al. 2021a; Pilguj et al. 2022). Increases in EML days appeared to be driven by warming and drying trends in the western and southwestern CONUS over the study period, resulting in warmer surface temperatures and steeper PBL lapse rates which were subsequently advected downstream. Significant increases in EML base temperatures and EML lapse rates resulted, with the increased lapse rates supporting higher EML frequency. Warmer EML bases also significantly increased the absolute MLCIN associated with EMLs, which appeared to have implications for CI (Taszarek et al. 2021a). Although this study did not do a comprehensive evaluation of the low-level or midlevel winds associated with the EML, they enable EML formation via the advection of warm, well-mixed PBLs off of the high terrain. Thus, trends such as stronger or more westerly winds within the period could have played a supporting role in the increased frequency of the EML. To determine if the trends in EML days and their attributes are persistent or relatively recent developments, future work could extend the study period, since ERA5 is now available to 1940. Additional work could also examine the impact of drought on EML frequency to determine if warm seasons with, or proceeded by, exceptionally dry conditions in the western CONUS saw increased EML occurrence. Finally, because continued trends toward more EMLs and stronger inhibition would have substantial implications for future thunderstorm frequency and intensity (e.g., Rasmussen et al. 2020; Taszarek et al. 2021a; Haberlie et al. 2022; Ashley et al. 2023), similar methodology could be applied to climate simulations to examine future projections of the EML and its capping inversion.

Acknowledgments. The authors thank Dr. Aaron Kennedy and two anonymous reviewers for their comments and suggestions that greatly improved the manuscript. This work was supported by grants from the National Science Foundation (Award 2048770) and the Polish National Science Center (Project 2020/39/D/ST10/00768).

Data availability statement. ERA5 data were downloaded from the ECMWF Copernicus Climate Change Service, available at https://cds.climate.copernicus.eu/.

REFERENCES

Agard, V., and K. Emanuel, 2017: Clausius–Clapeyron scaling of peak CAPE in continental convective storm environments. *J. Atmos. Sci.*, **74**, 3043–3054, https://doi.org/10.1175/JAS-D-16-0352.1.

Arritt, R. W., J. M. Wilczak, and G. S. Young, 1992: Observations and numerical modeling of an elevated mixed layer. *Mon. Wea. Rev.*, **120**, 2869–2880, https://doi.org/10.1175/1520-0493(1992)120<2869:OANMOA>2.0.CO;2.

Ashley, W. S., A. M. Haberlie, and V. A. Gensini, 2023: The future of supercells in the United States. *Bull. Amer. Meteor. Soc.*, **104**, E1–E21, https://doi.org/10.1175/BAMS-D-22-0027.1.

Banacos, P. C., and M. L. Ekster, 2010: The association of the elevated mixed layer with significant severe weather events in the northeastern United States. *Wea. Forecasting*, **25**, 1082–1102, https://doi.org/10.1175/2010WAF2222363.1.

Benjamin, S. G., 1986: Some effects of surface heating and topography on the regional severe storm environment. Part II: Two-dimensional idealized experiments. *Mon. Wea. Rev.*, **114**, 330–343, https://doi.org/10.1175/1520-0493(1986)114<0330:SEOSHA>2.0.CO;2.

——, and T. N. Carlson, 1986: Some effects of surface heating and topography on the regional severe storm environment. Part I: Three-dimensional simulations. *Mon. Wea. Rev.*, **114**, 307–329, https://doi.org/10.1175/1520-0493(1986)114<0307:SEOSHA>2.0.CO;2.

Brooks, H. E., 2009: Proximity soundings for severe convection for Europe and the United States from reanalysis data. *Atmos. Res.*, **93**, 546–553, https://doi.org/10.1016/j.atmosres.2008.10.005.

——, J. W. Lee, and J. P. Craven, 2003: The spatial distribution of severe thunderstorm and tornado environments from global reanalysis data. *Atmos. Res.*, **67–68**, 73–94, https://doi.org/10.1016/S0169-8095(03)00045-0.

Bunkers, M. J., J. R. Wetenkamp Jr., J. J. Schild, and A. Fischer, 2010: Observations of the relationship between 700-mb temperatures and severe weather reports across the contiguous United States. *Wea. Forecasting*, **25**, 799–814, https://doi.org/10.1175/2009WAF2222333.1.

Carlson, T. N., and F. H. Ludlam, 1968: Conditions for the occurrence of severe local storms. *Tellus*, **20A**, 203–226, https://doi.org/10.3402/tellusa.v20i2.10002.

——, S. G. Benjamin, G. S. Forbes, and Y.-F. Li, 1983: Elevated mixed layers in the regional severe storm environment: Conceptual model and case studies. *Mon. Wea. Rev.*, **111**, 1453–1474, https://doi.org/10.1175/1520-0493(1983)111<1453:EMLITR>2.0.CO;2.

Copernicus Climate Change Service, 2017: ERA5: Fifth generation of ECMWF atmospheric reanalyses of the global climate. Copernicus Climate Change Service Climate Data Store (CDS), accessed December 2021, https://cds.climate.copernicus.eu/cdsapp#!/dataset/reanalysis-era5-complete?tab=overview.

Cordeira, J. M., N. D. Metz, M. E. Howarth, and T. J. Galarneau Jr., 2017: Multiscale upstream and in situ precursors to the elevated mixed layer and high-impact weather over the Midwest United States. *Wea. Forecasting*, **32**, 905–923, https://doi.org/10.1175/WAF-D-16-0122.1.

Doswell, C. A., III, and E. N. Rasmussen, 1994: The effect of neglecting the virtual temperature correction on CAPE calculations. *Wea. Forecasting*, **9**, 625–629, https://doi.org/10.1175/1520-0434(1994)009<0625:TEONTV>2.0.CO;2.

Emanuel, K., 2023: On the physics of high CAPE. *J. Atmos. Sci.*, **80**, 2669–2683, https://doi.org/10.1175/JAS-D-23-0060.1.

Farrell, R. J., and T. N. Carlson, 1989: Evidence for the role of the lid and underrunning in an outbreak of tornadic thunderstorms. *Mon. Wea. Rev.*, **117**, 857–871, https://doi.org/10.1175/1520-0493(1989)117<0857:EFTROT>2.0.CO;2.

Fawbush, E. J., and R. C. Miller, 1954: The types of airmasses in which North American tornadoes form. *Bull. Amer. Meteor. Soc.*, **35**, 154–165, https://doi.org/10.1175/1520-0477-35.4.154.

Gensini, V. A., 2021: Severe convective storms in a changing climate. *Climate Change and Extreme Events*, A. Fares, Ed., Elsevier, 39–56.

——, and W. S. Ashley, 2011: Climatology of potentially severe convective environments from the North American regional reanalysis. *Electron. J. Severe Storms Meteor.*, **6** (8), https://doi.org/10.55599/ejssm.v6i8.35.

——, and T. L. Mote, 2015: Downscaled estimates of late 21st century severe weather from CCSM3. *Climatic Change*, **129**, 307–321, https://doi.org/10.1007/s10584-014-1320-z.

——, and H. E. Brooks, 2018: Spatial trends in United States tornado frequency. *npj Climate Atmos. Sci.*, **1**, 38, https://doi.org/10.1038/s41612-018-0048-2.

——, and L. Bravo de Guenni, 2019: Environmental covariate representation of seasonal U.S. tornado frequency. *J. Appl. Meteor. Climatol.*, **58**, 1353–1367, https://doi.org/10.1175/JAMC-D-18-0305.1.

——, T. L. Mote, and H. E. Brooks, 2014a: Severe-thunderstorm reanalysis environments and collocated radiosonde observations. *J. Appl. Meteor. Climatol.*, **53**, 742–751, https://doi.org/10.1175/JAMC-D-13-0263.1.

——, C. Ramseyer, and T. L. Mote, 2014b: Future convective environments using NARCCAP. *Int. J. Climatol.*, **34**, 1699–1705, https://doi.org/10.1002/joc.3769.

——, A. M. Haberlie, and P. T. Marsh, 2020: Practically perfect hindcasts of severe convective storms. *Bull. Amer. Meteor. Soc.*, **101**, E1259–E1278, https://doi.org/10.1175/BAMS-D-19-0321.1.

Graziano, T. M., and T. N. Carlson, 1987: A statistical evaluation of lid strength on deep convection. *Wea. Forecasting*, **2**, 127–139, https://doi.org/10.1175/1520-0434(1987)002<0127:ASEOLS>2.0.CO;2.

Haberlie, A. M., W. S. Ashley, C. M. Battisto, and V. A. Gensini, 2022: Thunderstorm activity under intermediate and extreme climate change scenarios. *Geophys. Res. Lett.*, **49**, e2022GL098779, https://doi.org/10.1029/2022GL098779.

Hersbach, H., and Coauthors, 2020: The ERA5 global reanalysis. *Quart. J. Roy. Meteor. Soc.*, **146**, 1999–2049, https://doi.org/10.1002/qj.3803.

Hoogewind, K. A., M. E. Baldwin, and R. J. Trapp, 2017: The impact of climate change on hazardous convective weather in the United States: Insight from high-resolution dynamical downscaling. *J. Climate*, **30**, 10 081–10 100, https://doi.org/10.1175/JCLI-D-16-0885.1.

IPCC, 2022: *Climate Change 2022: Impacts, Adaptation and Vulnerability*. Cambridge University Press, 3056 pp.

Johns, R. H., and C. A. Doswell III, 1992: Severe local storms forecasting. *Wea. Forecasting*, **7**, 588–612, https://doi.org/10.1175/1520-0434(1992)007<0588:SLSF>2.0.CO;2.

Keyser, D., and T. N. Carlson, 1984: Transverse ageostrophic circulations associated with elevated mixed layers. *Mon. Wea. Rev.*, **112**, 2465–2478, https://doi.org/10.1175/1520-0493(1984)112<2465:TACAWE>2.0.CO;2.

King, A. T., and A. D. Kennedy, 2019: North American supercell environments in atmospheric reanalyses and RUC-2. *J. Appl. Meteor. Climatol.*, **58**, 71–92, https://doi.org/10.1175/JAMC-D-18-0015.1.

Lanicci, J. M., and T. T. Warner, 1991a: A synoptic climatology of the elevated mixed-layer inversion over the Southern Great Plains in spring. Part I: Structure, dynamics, and seasonal evolution. *Wea. Forecasting*, **6**, 181–197, https://doi.org/10.1175/1520-0434(1991)006<0181:ASCOTE>2.0.CO;2.

——, and ——, 1991b: A synoptic climatology of the elevated mixed-layer inversion over the Southern Great Plains in spring. Part II: The life cycle of the lid. *Wea. Forecasting*, **6**, 198–213, https://doi.org/10.1175/1520-0434(1991)006<0198:ASCOTE>2.0.CO;2.

——, and ——, 1991c: A synoptic climatology of the elevated mixed-layer inversion over the Southern Great Plains in spring. Part III: Relationship to severe-storms climatology. *Wea. Forecasting*, **6**, 214–226, https://doi.org/10.1175/1520-0434(1991)006<0214:ASCOTE>2.0.CO;2.

——, T. N. Carlson, and T. T. Warner, 1987: Sensitivity of the Great Plains severe-storm environment to soil-moisture distribution. *Mon. Wea. Rev.*, **115**, 2660–2673, https://doi.org/10.1175/1520-0493(1987)115<2660:SOTGPS>2.0.CO;2.

Li, F., D. R. Chavas, K. A. Reed, and D. T. Dawson II, 2020: Climatology of severe local storm environments and synoptic-scale features over North America in ERA5 reanalysis and CAM6 simulation. *J. Climate*, **33**, 8339–8365, https://doi.org/10.1175/JCLI-D-19-0986.1.

——, ——, ——, N. Rosenbloom, and D. T. Dawson II, 2021: The role of elevated terrain and the Gulf of Mexico in the production of severe local storm environments over North

America. *J. Climate*, **34**, 7799–7819, https://doi.org/10.1175/JCLI-D-20-0607.1.

McNulty, R. P., 1985: A conceptual approach to thunderstorm forecasting. *Natl. Wea. Dig.*, **10** (2), 26–30.

——, 1995: Severe and convective weather: A central region forecasting challenge. *Wea. Forecasting*, **10**, 187–202, https://doi.org/10.1175/1520-0434(1995)010<0187:SACWAC>2.0.CO;2.

Molina, M. J., and J. T. Allen, 2019: On the moisture origins of tornadic thunderstorms. *J. Climate*, **32**, 4321–4346, https://doi.org/10.1175/JCLI-D-18-0784.1.

NOAA, 2023: Climate at a glance: Regional time series. NOAA/National Centers for Environmental Information, accessed April 2023, https://www.ncei.noaa.gov/access/monitoring/climate-at-a-glance/regional/time-series/107/pdsi/all/1/1979-2021.

Pilguj, N., M. Taszarek, J. T. Allen, and K. A. Hoogewind, 2022: Are trends in convective parameters over the United States and Europe consistent between reanalyses and observations? *J. Climate*, **35**, 3605–3626, https://doi.org/10.1175/JCLI-D-21-0135.1.

Rasmussen, E. N., and D. O. Blanchard, 1998: A baseline climatology of sounding-derived supercell and tornado forecast parameters. *Wea. Forecasting*, **13**, 1148–1164, https://doi.org/10.1175/1520-0434(1998)013<1148:ABCOSD>2.0.CO;2.

Rasmussen, K. L., A. F. Prein, R. M. Rasmussen, K. Ikeda, and C. Liu, 2020: Changes in the convective population and thermodynamic environments in convection-permitting regional climate simulations over the United States. *Climate Dyn.*, **55**, 383–408, https://doi.org/10.1007/s00382-017-4000-7.

Ribeiro, B. Z., and L. F. Bosart, 2018: Elevated mixed layers and associated severe thunderstorm environments in South and North America. *Mon. Wea. Rev.*, **146**, 3–28, https://doi.org/10.1175/MWR-D-17-0121.1.

Riemann-Campe, K., K. Fraedrich, and F. Lunkeit, 2009: Global climatology of Convective Available Potential Energy (CAPE) and Convective Inhibition (CIN) in ERA-40 reanalysis. *Atmos. Res.*, **93**, 534–545, https://doi.org/10.1016/j.atmosres.2008.09.037.

Saha, S., and Coauthors, 2010: The NCEP Climate Forecast System Reanalysis. *Bull. Amer. Meteor. Soc.*, **91**, 1015–1058, https://doi.org/10.1175/2010BAMS3001.1.

Seager, R., N. Lis, J. Feldman, M. Ting, A. P. Williams, J. Nakamura, H. Liu, and N. Henderson, 2018: Whither the 100th meridian? The once and future physical and human geography of America's arid–humid divide. Part I: The story so far. *Earth Interact.*, **22**, https://doi.org/10.1175/EI-D-17-0011.1.

Tang, B. H., V. A. Gensini, and C. R. Homeyer, 2019: Trends in United States large hail environments and observations. *npj Climate Atmos. Sci.*, **2**, 45, https://doi.org/10.1038/s41612-019-0103-7.

Taszarek, M., H. E. Brooks, B. Czernecki, P. Szuster, and K. Fortuniak, 2018: Climatological aspects of convective parameters over Europe: A comparison of ERA-Interim and sounding data. *J. Climate*, **31**, 4281–4308, https://doi.org/10.1175/JCLI-D-17-0596.1.

——, J. T. Allen, T. Púčik, K. A. Hoogewind, and H. E. Brooks, 2020: Severe convective storms across Europe and the United States. Part II: ERA5 environments associated with lightning, large hail, severe wind, and tornadoes. *J. Climate*, **33**, 10 263–10 286, https://doi.org/10.1175/JCLI-D-20-0346.1.

——, ——, H. E. Brooks, N. Pilguj, and B. Czernecki, 2021a: Differing trends in United States and European severe thunderstorm environments in a warming climate. *Bull. Amer. Meteor. Soc.*, **102**, E296–E322, https://doi.org/10.1175/BAMS-D-20-0004.1.

——, N. Pilguj, J. T. Allen, V. Gensini, H. E. Brooks, and P. Szuster, 2021b: Comparison of convective parameters derived from ERA5 and MERRA-2 with rawinsonde data over Europe and North America. *J. Climate*, **34**, 3211–3237, https://doi.org/10.1175/JCLI-D-20-0484.1.

Tuckman, P., V. Agard, and K. Emanuel, 2023: Evolution of convective energy and inhibition before instances of large CAPE. *Mon. Wea. Rev.*, **151**, 321–338, https://doi.org/10.1175/MWR-D-21-0302.1.

Weckwerth, T. M., and D. B. Parsons, 2006: A review of convection initiation and motivation for IHOP_2002. *Mon. Wea. Rev.*, **134**, 5–22, https://doi.org/10.1175/MWR3067.1.

Wilcox, R. R., 2010: *Fundamentals of Modern Statistical Methods: Substantially Improving Power and Accuracy*. Springer, 249 pp.

Zhang, L. N., D. J. Short Gianotti, and D. Entekhabi, 2023: Land surface influence on convective available potential energy (CAPE) change during interstorms. *J. Hydrometeor.*, **24**, 1365–1376, https://doi.org/10.1175/JHM-D-22-0191.1.